J. Rosato et al.

Design of a hybrid Monte Carlo method for line radiation transport simulations in magnetic fusion

Design of a hybrid Monte Carlo method for line radiation transport simulations in magnetic fusion

J. Rosato[1], Y. Marandet[1], D. Reiter[2] and R. Stamm[1]

[1]*Aix-Marseille Université, CNRS, PIIM UMR 7345, 13397 Marseille Cedex 20, France*
[2]*IEK-4 Plasmaphysik, Forschungszentrum Jülich GmbH, Trilateral Euregio Cluster, 52425 Jülich, Germany*

We report on a kinetic transport model for the Lyman line radiation in optically thick divertor plasma conditions encountered in exhaust systems in magnetic fusion devices. The model employs a modified kinetic Monte Carlo method designed to switch automatically between a true random walk and an effective one, which employs an ad hoc evaluation of the collision number in highly scattering regions. The method is suggested as a simple candidate for speeding up the kinetic transport codes currently involved in magnetic fusion research for ITER and DEMO divertor (power and particle exhaust system) design, without invoking the computationally more complex multiple scattering theories nor fully implementing the hybrid transport (discrete) diffusion Monte Carlo schemes (DDMC). Prototypical applications in one- and two-dimensional slab geometry are performed as an illustration.

-----

1) Introduction

Radiation transport can be important in magnetic fusion devices, in particular in the divertor region were a cold, dense and chemically rich plasma in recombining regime (typically $T_e < 5$ eV, $N_e > 10^{14}$ cm^{-3}) is opaque to the first Lyman lines of the hydrogen isotopes. Opacity effects in high density / large size divertor plasmas have been demonstrated, in accordance with photon mean free path estimates in the millimeter range [1], experimentally [2] and numerically [3–5]. A consequence of the line opacity is that the corresponding photoexcitation may significantly affect the ionization-recombination balance of the edge plasma. The preparation of operation and interpretation of large-scale fusion reactor devices (ITER, DEMO) requires accurate transport models for the plasma edge able to account for neutral and charged particles, together with line radiation, in a self-consistent fashion. For certain divertor configurations, the run time in in such non-linearly coupled fully kinetic transport codes is currently reported to be so large that it rules out any practical analysis of analogue results when extrapolating beyond ITER, e.g. towards conventional detached DEMO divertor scenarios [6]. In its current version, the radiation transport model used in B2-EIRENE [7,8] involves the kinetic radiative transfer equation and this equation is solved using a conventional Monte Carlo method, in the same way as the Boltzmann equation for neutrals (atoms, molecules) is solved. In this work, we report on the development of a hybrid scheme designed to switch automatically between a true random walk and an effective one, which employs an ad hoc evaluation of the collision number in highly scattering regions. Although not strictly necessary, but for simplifying the presentation, we adopt a collision (rather than track length) estimator also for the region in which the full random walk is retained. The theoretical framework of kinetic radiative transfer modeling, together with the conventional Monte Carlo terminology from linear transport applications used in EIRENE, are introduced in Sec. 2. The effective collision estimator is introduced in Sec. 3 and the hybrid method that switches between the two estimators is next presented in Sec. 3. Applications to slab geometry are performed as an illustration.

2) Monte Carlo formulation of line radiation transport

Specifically, we consider hereafter the transport of hydrogen Lyman photons in an optically thick divertor plasma. For our purposes it will be sufficient to focus on the time-independent radiative transfer problem. The radiative transfer equation in stationary regime takes the form of a kinetic Boltzmann equation

$$[\mathbf{\Omega} \cdot \nabla + \Sigma_t(x)]F(x) = \int d^3E' C(\mathbf{E}, \mathbf{E}'; \mathbf{r})\Sigma_t(\mathbf{r}, \mathbf{E}')F(\mathbf{r}, \mathbf{E}') + Q(x). \tag{1}$$

Notations similar to those in the literature on Monte Carlo particle transport methods [9,10] are used here: $F(\mathbf{r},\mathbf{E}) \equiv F(x)$ denotes the photon flux ($m^{-2} \times s^{-1} \times J^{-1} \times sr^{-1}$); x is a shortcut for the phase space coordinates $(\mathbf{r},\mathbf{E})$ with $\mathbf{E} = E\mathbf{\Omega}$, $E = |\mathbf{E}|$ being the photon energy and $\mathbf{\Omega}$ giving the propagation direction; $\Sigma_t(x)$ is the total macroscopic cross section (m^{-1}) comprising photon absorption and scattering; $C(\mathbf{E},\mathbf{E}';\mathbf{r})$ denotes a collision kernel for photon scattering by atoms, which describes an energy-momentum transfer from $\mathbf{E}'$ to $\mathbf{E}$ (note the order of arguments used in [9] is the opposite to that used here); and $Q(x)$ is a source density corresponding to spontaneous emission. Equation (1) is equivalent to the radiative transfer equation used in spectroscopy and astrophysics (e.g. [11–13]). The photon flux is proportional to the specific intensity

$$F(x) = \frac{I(\mathbf{r}, \mathbf{\Omega}, \nu = E/h)}{Eh}. \tag{2}$$

The macroscopic cross section corresponds to the so-called extinction coefficient; it is given in terms of the Einstein B coefficient as

$$\Sigma_t(x) = \frac{E_{n1}}{4\pi} N_1(\mathbf{r})B_{1n}\phi(\nu; \mathbf{r}, \mathbf{\Omega}), \tag{3}$$

or, alternatively,

$$\Sigma_t(x) = N_1(\mathbf{r})\sigma(x), \tag{4}$$

$$\sigma(x) = \frac{r_e c f_{1n}}{4}\phi(\nu; \mathbf{r}, \mathbf{\Omega}), \tag{5}$$

where σ denotes the microscopic cross section, written here in terms of the oscillator strength $f_{1n} \equiv E_{n1}B_{1n}/\pi r_e c$ (e.g. [14]). The classical electron radius $r_e = e^2/4\pi\varepsilon_0 m_e c^2$ has been introduced for notational simplicity sake. N_1 denotes the density of absorbers (i.e., atoms in the ground state), $E_{n1} = E_n - E_1$ is the difference between the upper and lower energy level energies (n being the principal quantum number of the upper level), and ϕ is the probability density for absorbing a photon with frequency ν conditioned to the position $\mathbf{r}$ and direction $\mathbf{\Omega}$; it is referred to as the spectral line shape function and its structure depends on the physical processes that occur at the microscopic scale (Stark and Zeeman effects, Doppler broadening). A more comprehensive discussion of the line broadening mechanisms in optically thick divertor conditions can be found in [15]. The source $Q(x)$ present in the right-hand side of the transport equation (1) has a structure similar to the macroscopic cross section: it is proportional to the line shape function and it involves the A Einstein coefficient relative to spontaneous emission:

$$Q(x) = \frac{1}{4\pi h} N_n^*(\mathbf{r})A_{n1}\phi(\nu; \mathbf{r}, \mathbf{\Omega}), \tag{6}$$

Here, N_n^* denotes the density of atoms excited to level n due to processes other than photon absorption, and A_{n1} is related to f_{1n} via $A_{n1} = (g_1/g_n)2\pi\nu_{n1}^2 r_e f_{1n}/c$ with $\nu_{n1} = E_{n1}/h$ and where g_1, g_n denote the statistical weight of the lower and upper level, respectively. The collision kernel $C(\mathbf{E},\mathbf{E}';\mathbf{r})$ in Eq. (1) is proportional to the conditional probability density of photon emission with energy-momentum $\mathbf{E}$ given an incoming photon at $\mathbf{r}$ with energy-momentum $\mathbf{E}'$. It is normalized to the total probability of scattering

$$\int d^3E\, C(\mathbf{E}, \mathbf{E}'; \mathbf{r}) = p_s(\mathbf{r}) \leq 1, \tag{7}$$

and the latter can be described as a branching ratio qualifying the relative contribution of spontaneous emission with respect to all processes depopulating the excited level n

$$p_s = \frac{A_{n1}}{A_{n1} + \Gamma_n}. \tag{8}$$

Here, Γ_n denotes the total rate of processes other than spontaneous emission (collisional excitation, ionization etc.) that depopulate the level n. The product $p_s \times \Sigma_t \equiv \Sigma_s$ can be interpreted as a macroscopic cross section for scattering. (Hence, in our context, a scattering event is the sequence of photon absorption and instantaneous spontaneous emission; such a combined treatment of absorption and emission as "scattering" is the key idea of the so called implicit Monte Carlo scheme in radiative transfer applications.) The energy dependence of the collision kernel depends on the physical processes that occur at the microscopic scale, in a way similar to that for the line shape function (Stark effect etc.). Models involve the so-called redistribution functions (or "two-photon" line shapes) and can be established using an appropriate extension of line shape models; e.g. [16] for an application to optically thick divertor plasma conditions. Note that the transport equation (1) does not account for stimulated emission, i.e., it is implied that no population inversion is present. In a more general case, this process can be retained through a negative contribution to the absorption cross section and, if the radiation field is strong, through additional scattering terms which are nonlinear in the radiation flux. The structure of the transport equation (1) makes it suitable for kinetic Monte-Carlo simulations involving random walks. We follow the terminology used in the EIRENE code and reported in the literature on neutron transport [9]. We define the photon collision density $\psi(x) = \Sigma_t(x)F(x)$ and we write an integral equation for it, from integration of Eq. (1) along the characteristics:

$$\psi(x) = \int d^6 x' K(x,x')\psi(x') + S(x). \tag{9}$$

The source S and the kernel K are given by

$$S(x) = \int d^3 r' T(\mathbf{r},\mathbf{r}';\mathbf{E})Q(\mathbf{r}',\mathbf{E}), \tag{10}$$

$$K(x,x') = T(\mathbf{r},\mathbf{r}';\mathbf{E})C(\mathbf{E},\mathbf{E}';\mathbf{r}'), \tag{11}$$

where $T(\mathbf{r},\mathbf{r}';\mathbf{E}) = \theta(\mathbf{\Omega}.(\mathbf{r} - \mathbf{r}'))\Sigma_t(x)\exp(-\int_0^{\mathbf{\Omega}.(\mathbf{r} - \mathbf{r}')}ds\Sigma_t(\mathbf{r}' + \mathbf{\Omega}s,\mathbf{E}))\delta(\mathbf{r}_\perp - \mathbf{r}'_\perp)$ denotes the conditional probability of a photon interacting with an atom (either through absorption or scattering) at $\mathbf{r}$; θ is the Heaviside function and $\perp$ refers to the plane perpendicular to $\mathbf{\Omega}$ (note the order of arguments here is also different to that in [9]). The quantities $p^1(x) = S(x)/\int d^6 x' Q(x')$, $p(x,x') = K(x,x')$, and $p(\mathbf{r}) = 1 - \int d^6 x' K(x',x)$ $= 1 - p_s(\mathbf{r})$ are directly interpretable as probabilities associated with a continuous random walk process $\alpha = (x_1...x_k)$. This allows one to evaluate physical observables by generating a set of random sequences and using an appropriate estimator. An example of such is the so-called collision estimator: given a detector function g(x), the integral $I_g = \int d^6 x g(x)\psi(x)$ is evaluated from the expectation value of the random variable $\eta(\alpha) = W \times \Sigma_{m=1}^k g(x_m)$, where $W \equiv \int d^6 x' Q(x')$ and the sum is performed over collisions. The collision estimator is suitable in particular for opaque regions where the photon mean free path Σ_t^{-1} is small. Variants can be used alternatively, e.g. the absorption estimator or the track length estimator. The latter, which is used by default in EIRENE, is most efficient in optically thin media where collisions are rare. For our purposes it suffices to state that the estimators yield the same result (all are unbiased).

3) An estimator for highly scattering regions

In optically thick divertor plasmas, the conditions are such that the probability of scattering is generally large while the mean free path of resonant (Lyman α) photons is small (see Fig. 1). Even though the Monte Carlo calculation yields a correct estimation of the responses to detector functions I_g, it requires the counting of a large number of collisions, which can be CPU intensive in a realistic geometry where the photons are generated and tracked along many cells. A modification of the estimator that provides the number of collisions in highly scattering regions without explicitly following the trajectories would be very beneficial; it is the subject of so-called multiple scattering theories also frequently derived for electron transport studies in solid or liquid targets. Here, we note that for our particular case a simple example of such an estimator is given by the geometric distribution: given a phase space cell j with high probability of scattering and small photon mean free path, the collisions that occur inside it can be

interpreted as Bernoulli trials for either leaving the cell and going to a neighboring one or for being absorbed. Each trial has a probability of "success" (namely, remaining in the cell without being absorbed) of $p_s(\mathbf{r}_j) \times p_{in}(x_j)$, where $p_{in}(x_j) = \int_{V_j} d^3 r T(\mathbf{r}, \mathbf{r}_j; E_j)$ is the probability of flight from $\mathbf{r}_j$ to any location inside the cell under consideration; the integral here is carried out on the cell volume V_j. An approximation for this quantity can be obtained by taking the $\Sigma_t \to \infty$ limit of the transport kernel. The following relation holds (see Appendix A)

$$T(\mathbf{r}, \mathbf{r}_j; E_j) \approx \left[1 - \frac{\mathbf{\Omega}_j \cdot \nabla}{\Sigma_t(x_j)} + \left(\frac{\mathbf{\Omega}_j \cdot \nabla}{\Sigma_t(x_j)} \right)^2 \right] \delta(\mathbf{r} - \mathbf{r}_j),$$ (12)

or, by discretization,

$$T(\mathbf{r}, \mathbf{r}_j; E_j) \approx \left[1 - \frac{2}{\Sigma_t(x_j)^2 \Delta s_j^2} \right] \delta(\mathbf{r} - \mathbf{r}_j)$$

$$+ \left[\frac{1}{\Sigma_t(x_j)^2 \Delta s_j^2} - \frac{1}{2\Sigma_t(x_j)\Delta s_j} \right] \delta(\mathbf{r} - \mathbf{r}_j + \mathbf{\Omega}_j \Delta s_j),$$ (13)

$$+ \left[\frac{1}{\Sigma_t(x_j)^2 \Delta s_j^2} + \frac{1}{2\Sigma_t(x_j)\Delta s_j} \right] \delta(\mathbf{r} - \mathbf{r}_j - \mathbf{\Omega}_j \Delta s_j)$$

where Δs_j stands for the distance between $\mathbf{r}_j$ and a point inside the nearest cell. Integrating Eq. (13) over the cell volume yields the following relation

$$\int_{V_j} d^3 r T(\mathbf{r}, \mathbf{r}_j; E_j) \approx \left[1 - \frac{2}{\Sigma_t(x_j)^2 \Delta s_j^2} \right],$$ (14)

which can be used for evaluating the probability $p_{in}(x_j)$. Note that the distance Δs_j depends on the position $\mathbf{r}_j$ prior to flight and, hence, so does the probability $p_{in}(x_j)$. A more practical model, with no explicit utilization of $\mathbf{r}_j$, consists in replacing Δs_j by an effective distance which only depends on the geometry of the cell under consideration. For example, if a mesh of rectangular cuboid shape $\Delta x \times \Delta y \times \Delta z$ is used, this distance can be evaluated by replacing the operator $(\mathbf{\Omega}_j \cdot \nabla)^2$ in Eq. (12) by its angular average $(1/3)\nabla^2$ and next discretizing the Laplacian; this procedure amounts to substituting $1/\Delta s_j^2$ in Eq. (14) by $(1/\Delta x^2 + 1/\Delta y^2 + 1/\Delta z^2)/3$ (in d-dimensional geometry, this generalizes into the substitutions $(\mathbf{\Omega}_j \cdot \nabla)^2 \to (1/d)\nabla^2$ and $\sum_{a=1}^{d}(1/\Delta x_a^2)/d$). In practice, a calculation using the modified random walk and estimator consists in performing a random walk with jumps between adjacent cells; the number of collisions in each cell j is generated according to the geometric distribution and an option for absorption is allowed in the case where $p_s(\mathbf{r}_j) < 1$. Figure 2 shows an example of result in one-dimensional (slab) geometry. The plot represents the mean number of collisions occurring in the cells. The space is discretized over a regular lattice of 100 segments of size Δx and the total size is $L = 100 \times \Delta x$. Perfectly absorbing walls are assumed, i.e., a photon is considered as being lost if it attains one of the two boundaries. Also, for the sake of simplicity, all photons are assumed to have the same energy. In the calculation, the source, the macroscopic cross section and the collision kernel were assumed space and angle independent and the probability of scattering was set equal to unity. The macroscopic cross section was set equal to $10/\Delta x$; this assumption yields a photon mean free path shorter than the cell size, which renders the modified estimator applicable here. The result from the standard collision estimator and from analytic solution (see Appendix B) are also shown in the figure. As can be seen, the results coincide well with each other. The two Monte Carlo calculations were performed on a laptop with a single thread assuming 10000 trajectories. The calculation using the collision estimator took almost 5 minutes while the calculation using the modified estimator took 10 seconds. The speed up is even more important if the simulation is run in two-

dimensional geometry. Simulations have been performed as a test in a rectangle of size 2L² assuming the same plasma conditions as above. The calculation using the collision estimator took more than ten minutes whereas the calculation using the modified estimator took only 10 seconds. As in the one-dimensional case, the results are close to each other (see Fig. 3).
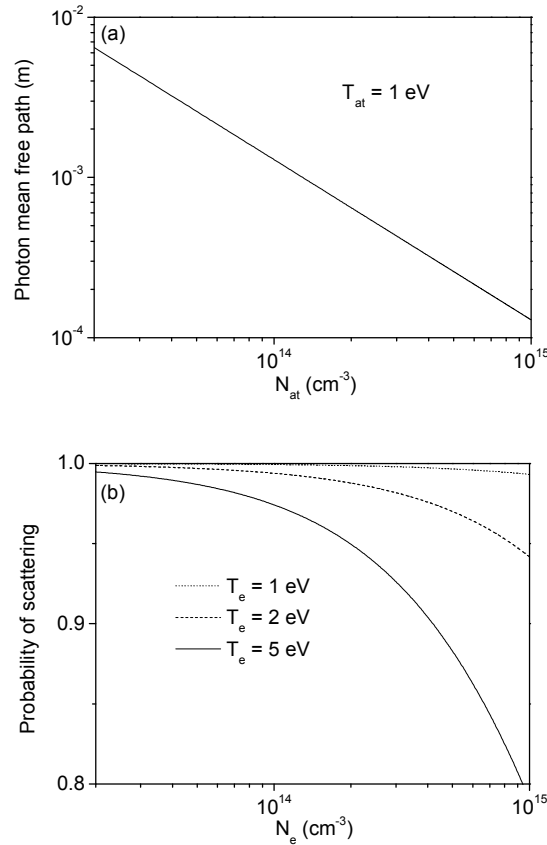

Figure 1 –Plot of (a) the Lyman α monochromatic photon mean free path Σ_t^{-1} at the Bohr frequency E_{21} and (b) the probability of scattering. The latter is estimated according to Eq. (8), retaining collisional deexcitation and collisional ionization from $n = 2$ as processes contributing to the rate Γ_2 (e.g. [17] for explicit formulas for these processes). A Gaussian line shape function accounting for Doppler broadening is assumed in the macroscopic cross section. As can be seen in the plots, the photon mean free path is shorter than 1 mm while the probability of scattering remains large at high density divertor plasma conditions.
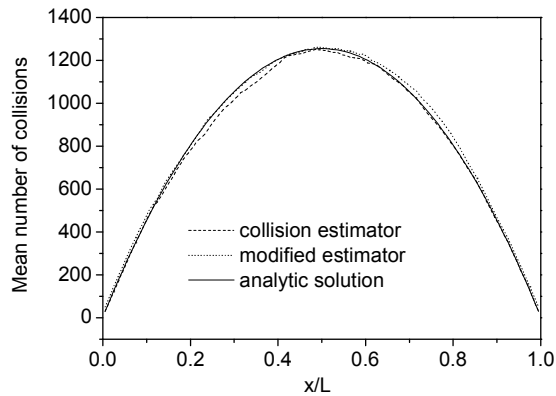
Figure 2 – Plot of the mean number of collisions calculated in a homogeneous slab with perfectly absorbing walls. Conditions such that the modified estimator is applicable were assumed: the probability of scattering was set equal to unity and a value of $10/\Delta x$ was chosen for the macroscopic cross section Σ_t. As can be seen, the result coincides with that obtained from the standard collision estimator. Also shown in the figure is the result obtained from the analytic solution, which serves as a reference.
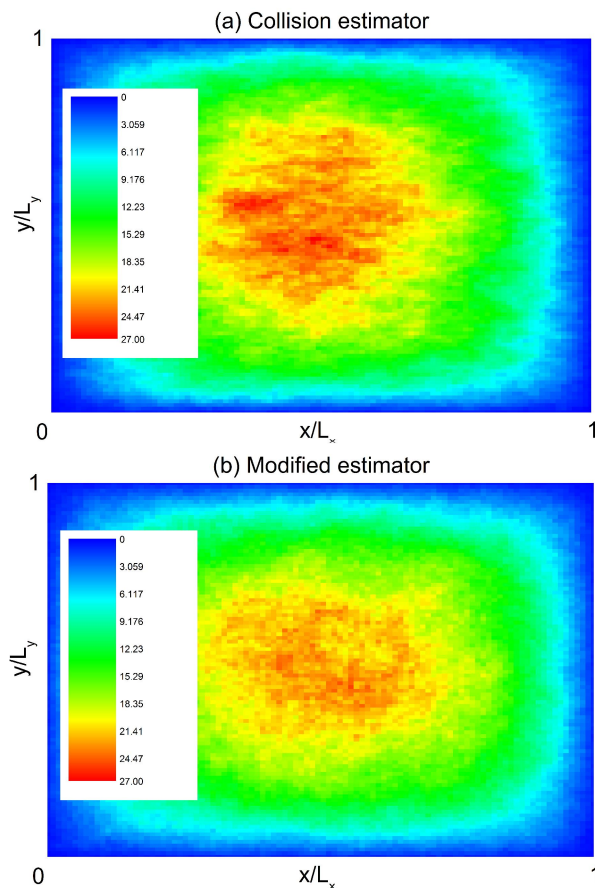

Figure 3 – Map of the mean collision number per cell calculated in a homogeneous rectangle. As in the one-dimensional case, the modified estimator (b) yields a result close to that obtained from the standard collision estimator (a).

4) Designing a hybrid estimator that switches between full and modified random walk

A hybrid scheme that switches between the true random walk and the modified one, according to the value of $\Sigma_t \Delta x$, would be very convenient for the design of future large scale devices such as ITER or DEMO that employs kinetic transport codes. Modeling efforts are presently ongoing in order to set up such a scheme (see [18,19] for recent works on radiative transfer); a noticeable issue is the description of the transition between these two estimators, namely, how to define a (mathematically) proper criterion for converting a "true" particle (in standard kinetic Monte Carlo terminology) into an "effective" one that evolves according to the modified random walk (and estimator) described in the previous section. Figure 4 shows an illustration of this issue. A hybrid simulation has been carried out in a slab of size L, assuming a linear spatial profile of Σ_t taking the values 100/L and 1000/L at the left and right boundaries, respectively, and assuming all other parameters homogeneous as in the previous section. A regular lattice of 100 segments of size $\Delta x = L/100$ has also been used. The criterion chosen here for using the modified estimator is that the product $\Sigma_t(x_j)\Delta x$ must be larger than 5. This roughly corresponds to the slab center. As can be seen in the figure, the result from the hybrid estimator is close to that obtained from the standard collision estimator (which serves as a reference here). The discontinuity that appears near the slab center corresponds to the boundary between the regions where the macroscopic cross section is small (left side) and large (right side). The bump visible on the right side, which denotes a large number of collisions owing to the shorter photon mean free path values in this region, is qualitatively well reproduced by the hybrid method. A gain of CPU time by a factor larger than 4 was obtained.
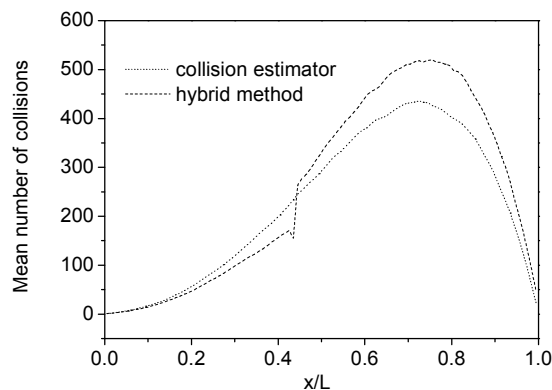

Figure 4 – Plot of the mean number of collisions calculated in a slab with linearly increasing macroscopic cross section. The bump present on the right side corresponds to a region where the photon mean free path is small. The hybrid method qualitatively well reproduces the result from the collision estimator. The discontinuity near the center, which is a feature of the hybrid method, corresponds to the interface between the region where the collision estimator is used (left side) and the region where the modified estimator is used (right side).

4) Conclusion

In the framework of tokamak edge plasma modeling, we have examined the feasibility of a hybrid transport model for line radiation, able to switch automatically between a true kinetic random walk where the number of collisions is counted along the full random flight and an effective one that provides the number of collisions in highly scattering regions without explicitly following the trajectories. A criterion that allows one to discriminate between the two kinds of random walks and their related collision estimators is provided by the ratio between the photon mean free path and the cell's characteristic size. The issue of properly interfacing between the kinetic and fluid zones is still pending. The results obtained

in our study have the correct order of magnitude but are dependent on the geometry under consideration. New calculations will be performed and confronted to analytical results (in particular, the issue of modeling the modified estimator is related to the "first-passage" problem, e.g. [20]). A further extension of this work will also concern the energy dependence of the various rates entering the transport equation. This will require the use of spectroscopic modeling techniques along the lines of those used in previous studies [15,16].

Appendix A

Consider the transport kernel in a region where the mean free path is much shorter than the characteristic gradient length of all other quantities. In this framework, the spatial dependence of the macroscopic cross section can be neglected and the following approximation holds

$$T(\mathbf{r},\mathbf{r'}) \approx \theta(\mathbf{\Omega}\cdot(\mathbf{r}-\mathbf{r'}))\Sigma_t(\mathbf{r'})e^{-\Sigma_t(\mathbf{r'})\mathbf{\Omega}\cdot(\mathbf{r}-\mathbf{r'})}\delta(\mathbf{r}_\perp - \mathbf{r'}_\perp) . \qquad (A1)$$

The energy dependence has not been written here for the sake of simplicity. Fourier transforming with respect to $\mathbf{r}$ yields

$$\hat{T}(\mathbf{k},\mathbf{r'}) \equiv \int d^3r e^{-i\mathbf{k}\cdot\mathbf{r}}T(\mathbf{r},\mathbf{r'}) \approx \frac{e^{-i\mathbf{k}\cdot\mathbf{r'}}}{1+i\mathbf{k}\cdot\mathbf{\Omega}/\Sigma_t(\mathbf{r'})} . \qquad (A2)$$

A Taylor expansion with respect to the variable $i\mathbf{k}.\mathbf{\Omega}/\Sigma_t(\mathbf{r'})$ can be performed in accordance to the short mean free path assumption:

$$\hat{T}(\mathbf{k},\mathbf{r'}) \approx e^{-i\mathbf{k}\cdot\mathbf{r'}}\left(1 - \frac{i\mathbf{k}\cdot\mathbf{\Omega}}{\Sigma_t(\mathbf{r'})} + \left(\frac{i\mathbf{k}\cdot\mathbf{\Omega}}{\Sigma_t(\mathbf{r'})}\right)^2\right) . \qquad (A3)$$

Equation (12) is obtained by inverse Fourier transform, i.e., formally, by performing the substitutions $i\mathbf{k} \leftrightarrow \nabla$ and $e^{-i\mathbf{k}.\mathbf{r'}} \leftrightarrow \delta(\mathbf{r}-\mathbf{r'})$.

Appendix B

The radiation transport equation in one-dimensional geometry, assuming all photons have the same energy and setting $p_s = 1$, has a simple analytic solution. The generic phase space coordinate $x \equiv (\mathbf{r},E)$ comes down to the pair (x,ε) where x now denotes one component of the position vector $\mathbf{r}$ and ε is the projection of $\mathbf{\Omega}$ onto the x axis, which is either equal to 1 or to -1. This simplification allows one to write the transport equation (1) as follows:

$$\left[\varepsilon\frac{d}{dx} + \Sigma_t(x)\right]F_\varepsilon(x) = \sum_{\varepsilon'}\frac{1}{2}\Sigma_t(x)F_{\varepsilon'}(x) + Q(x) . \qquad (B1)$$

The ε dependence has been written as an index, and it is implied here that neither the macroscopic cross section nor the source depend on the photon direction, i.e., the medium is assumed isotropic. In matrix form, equation (B1) reads:

$$\frac{d}{dx}\begin{pmatrix} F_1(x) \\ F_{-1}(x) \end{pmatrix} = \begin{pmatrix} -\frac{1}{2}\Sigma_t(x) & \frac{1}{2}\Sigma_t(x) \\ -\frac{1}{2}\Sigma_t(x) & \frac{1}{2}\Sigma_t(x) \end{pmatrix}\begin{pmatrix} F_1(x) \\ F_{-1}(x) \end{pmatrix} + \begin{pmatrix} Q(x) \\ -Q(x) \end{pmatrix}.$$ (B2)

$$\equiv M(x)\begin{pmatrix} F_1(x) \\ F_{-1}(x) \end{pmatrix} + P(x)$$

This equation can be solved in the same way as an ordinary differential equation on a commutative field because the square matrix M(x) commutes with itself at different values of x. The solution over the interval [0,L] reads

$$\begin{pmatrix} F_1(x) \\ F_{-1}(x) \end{pmatrix} = e^{\int_0^x dx' M(x')}\begin{pmatrix} F_1(0) \\ F_{-1}(0) \end{pmatrix} + \int_0^x dx' e^{\int_{x'}^x dx'' M(x'')} P(x'),$$ (B3)

with

$$e^{\int_{x'}^x dx'' M(x'')} = \begin{pmatrix} 1 - \frac{1}{2}\tau(x,x') & \frac{1}{2}\tau(x,x') \\ -\frac{1}{2}\tau(x,x') & 1 + \frac{1}{2}\tau(x,x') \end{pmatrix},$$ (B4)

$$\tau(x,x') = \int_{x'}^x dx'' \Sigma_t(x'').$$ (B5)

Note, M is a nilpotent matrix of degree 2 and, hence, the exponential is a polynomial of first order with respect to the optical depth τ. The application considered in Sec. 3 concerns a homogeneous slab where both Σ_t and Q are space independent, and with no incoming radiation; in this framework, the optical depth is a first order polynomial, viz., $\tau(x,x') = \Sigma_t \times (x - x')$, and the boundary conditions $F_1(0) = 0 = F_{-1}(L) = 0$ hold. Algebraic manipulations yield the following expression

$$\begin{pmatrix} F_1(x) \\ F_{-1}(x) \end{pmatrix} = \begin{pmatrix} \frac{1}{2}\Sigma_t x \\ 1 + \frac{1}{2}\Sigma_t x \end{pmatrix} F_{-1}(0) + Q\begin{pmatrix} x - \Sigma_t \frac{x^2}{2} \\ -x - \Sigma_t \frac{x^2}{2} \end{pmatrix}.$$ (B6)

The constant $F_{-1}(0)$ can be calculated from the condition $F_{-1}(L) = 0$, taking the second line of Eq. (B6) and replacing x by L; explicitly, one obtains $F_{-1}(0) = QL$. This expression was used in the plot presented in Fig. 2. The collision density summed over the directions $\varepsilon = \pm 1$ and integrated over a cell $[x_j, x_{j+1}]$ reads

$$\int_{x_j}^{x_{j+1}} dx \sum_\varepsilon \psi_\varepsilon(x) \equiv \int_{x_j}^{x_{j+1}} dx \sum_\varepsilon \Sigma_t F_\varepsilon(x)$$

$$= Q\Sigma_t L \int_{x_j}^{x_{j+1}} dx\left[1 + \Sigma_t x - \frac{\Sigma_t x^2}{L}\right].$$ (B7)

$$= Q\Sigma_t L\left[x + \frac{\Sigma_t x^2}{2} - \frac{\Sigma_t x^3}{3L}\right]_{x_j}^{x_{j+1}}$$

The normalization used in the plot corresponds to Q = 1/2L.

References

[1] D. E. Post, J. Nucl. Mater. 220-222, 143 (1995).
[2] J. L. Terry et al., Phys. Plasmas 5, 1759 (1998).
[3] H. A. Scott and M. L. Adams, Contrib. Plasma Phys. 44, 51 (2004).

[4] V. Kotov et al., Contrib. Plasma Phys. 46, 635 (2006).

[5] E. Marenkov, S. Krasheninnikov, and A. Pshenov, Contrib. Plasma Phys., in press.

[6] A. S. Kukushkin et al., Fusion Eng. Des. 86, 2865 (2011).

[7] D. Reiter, S. Wiesen, and M. Born, Plasma Phys. Control. Fusion 44, 1723 (2002).

[8] D. Reiter, M. Baelmans, and P. Börner, Fusion Sci. Technol. 47, 172 (2005); www.eirene.de

[9] J. Spanier and E. M. Gelbard, Monte Carlo Principles and Neutron Transport Problems (Dover, Mineola, 2008).

[10] I. Lux and L. Koblinger, Monte Carlo Particle Transport Methods: Neutron and Photon Calculations (CRC Press, Boca Raton, 1991).

[11] S. Chandrasekhar, Radiative Transfer (Dover, New York, 1960).

[12] D. Mihalas, Stellar Atmospheres (W. H. Freeman and Company, San Fransisco, 1978).

[13] J. Oxenius, Kinetic Theory of Particles and Photons – Theoretical Foundations of Non-LTE Plasma Spectroscopy (Springer, Berlin, 1986).

[14] G. C. Pomraning, The Equations of Radiation Hydrodynamics (Pergamon, Oxford, 1973).

[15] J. Rosato et al., Contrib. Plasma Phys. 50, 398 (2010).

[16] J. Rosato et al., J. Phys. B: At. Mol. Opt. Phys. 41, 165701 (2008).

[17] L. C. Johnson, Astrophys. J. 174, 227 (1972).

[18] J. Rosato et al., Contrib. Plasma Phys. 56, 663 (2016).

[19] J. Rosato et al., High Energy Density Phys. 22, 73 (2017).

[20] A. Zoia, E. Dumonteil, and A. Mazzolo, Phys. Rev. E 83, 041137 (2011).